Coverage-Dependent CO Adsorption Energy from First-Principles Calculations

Bin Shan,*,† Yujun Zhao,† Jangsuk Hyun,† Neeti Kapur,† John B. Nicholas,† and Kyeongjae Cho*,‡

Nanostellar Inc., 3696 Haven Avenue, Redwood City, California 94063, and Department of Materials Science and Engineering and Department of Physics, University of Texas at Dallas, Richardson, Texas 75080

Received: October 27, 2008; Revised Manuscript Received: December 24, 2008

CO saturation coverage on Pt(111) is crucially important in diesel oxidation catalysis. We systematically studied coverage-dependent CO adsorption on the Pt(111) surface using density functional theory (DFT) calculations and classical Monte-Carlo (MC) simulations. The zero-coverage-limit CO-adsorption energies at different binding sites are almost degenerate at the revised Perdew−Burke−Erzernhof functional (RPBE) level. As the CO coverage increases, strong through-space repulsion and substrate-mediated metal-sharing effects tend to dominate the stability of adsorbates and alter their binding preferences. The calculated differential binding energy curve and adsorption patterns compare well with experiments.

Introduction

CO oxidation on transition metal surfaces forms the basis for the catalytic CO removal from car exhaust gases. Platinum (Pt) is among one of the most active and widely used transition metal catalysts for CO oxidation. It has also been used as a benchmark system for fundamental studies of CO oxidation. The commonly accepted Langmuir−Hinshelwood mechanism for CO oxidation on Pt only involves a few elementary steps, including molecular CO adsorption and desorption, oxygen dissociation, and surface reaction of atomic oxygen with CO to form carbon dioxide. Under the high pressure conditions that are generally found in automotive catalytic converters, many reaction kinetic studies indicate a CO inhibition of O_2 dissociation, and the rate-limiting step in CO oxidation is CO desorption from the surface.[1,2] Because of the importance of CO adsorption in the overall oxidation process, many surface science measurements have been employed to investigate CO chemisorption in detail, including low energy electron diffraction (LEED),[3,4] electron energy loss spectroscopy (EELS),[5] and high pressure STM studies.[6,7]

On the theoretical side, CO binding energies have been explored on many transition metal surfaces.[5,8−12] In particular, CO adsorption on the Pt(111) surface has been extensively studied.[8,10−12] The accuracy of different exchange-correlation functionals in predicting CO binding energies on different adsorption sites was also evaluated.[9,13] Experimental results indicate that at low coverage, CO prefers to bind to top sites while DFT calculations consistently predict that CO prefers adsorption at hollow sites. The discrepancy is generally attributed to the overestimation of the HOMO−LUMO gap of CO.[9,13,14] A number of theoretical methods have been proposed to correct this problem.[14,15] Only very few theoretical studies have investigated the CO adsorption at high coverage. Hafner et al.[16] have studied CO adsorption with precovered CO molecules but only with a limited set of adsorption configurations.

In diesel engine catalysis under cold start conditions, the catalyst surface is initially saturated with CO molecules. The subsequent reactions, including oxygen dissociation and CO oxidation, take place on a CO covered surface. Because of this fundamental interest and technological importance, we sought to explore the coverage-dependent CO binding on Pt(111) and to determine the saturation coverage via DFT calculations.[17] By using DFT calculations and assisted by classical Monte-Carlo (MC) techniques, we report theoretically determined CO differential binding energy curve and saturation coverage on Pt(111). They both agree well with experiments and offer new insight to CO adsorption under realistic diesel engine operating conditions.

Computational Methods

The DFT calculations were done using the Vienna ab initio simulation package (VASP),[18] where Kohn−Sham single-electron wave functions are expanded by a series of plane waves. The interactions between ions and valence electrons are described using the projected augmented wave (PAW) method[19] with an energy cutoff of 400 eV, at which the CO binding energies are converged to a few millivolts. We used the revised Perdew−Burke−Erzernhof (RPBE)[20] functional, which produces good agreement with experimental adsorption energy values for a number of molecules on transition metal surfaces. The CO binding energies were calculated as the difference in total energy between the optimized Pt−CO complex and the sum of the energies of the optimized bare surface and gas-phase CO molecules:

$$\Delta E = E_{\text{total}} - (E_{\text{slab}} + nE_{\text{CO}}) \quad (1)$$

In order to probe complex CO equilibrium adsorption geometries at intermediate coverages, we used a p(4×4) unit cell (16 surface Pt atoms), with a $2 \times 2 \times 1$ k-point mesh to sample the Brillouin zone. The p(4×4) unit cell enables us to map out the differential binding energy curve in increments of 0.06 to 1.0 ML coverage. The Pt(111) substrate is modeled by a three-layer metal slab separated by a vacuum layer thickness of approximately 15 Å. The bottom layer of the slab is fixed in its crystallographic positions while the other atoms are free to relax.[8,10,11,21] We consider the geometry fully relaxed when the

* To whom correspondence should be addressed. E-mail: bshan@nanostellar.com; kjcho@utdallas.edu.
† Nanostellar Inc.
‡ University of Texas at Dallas.

10.1021/jp8094962 CCC: $40.75
Published on Web 03/24/2009

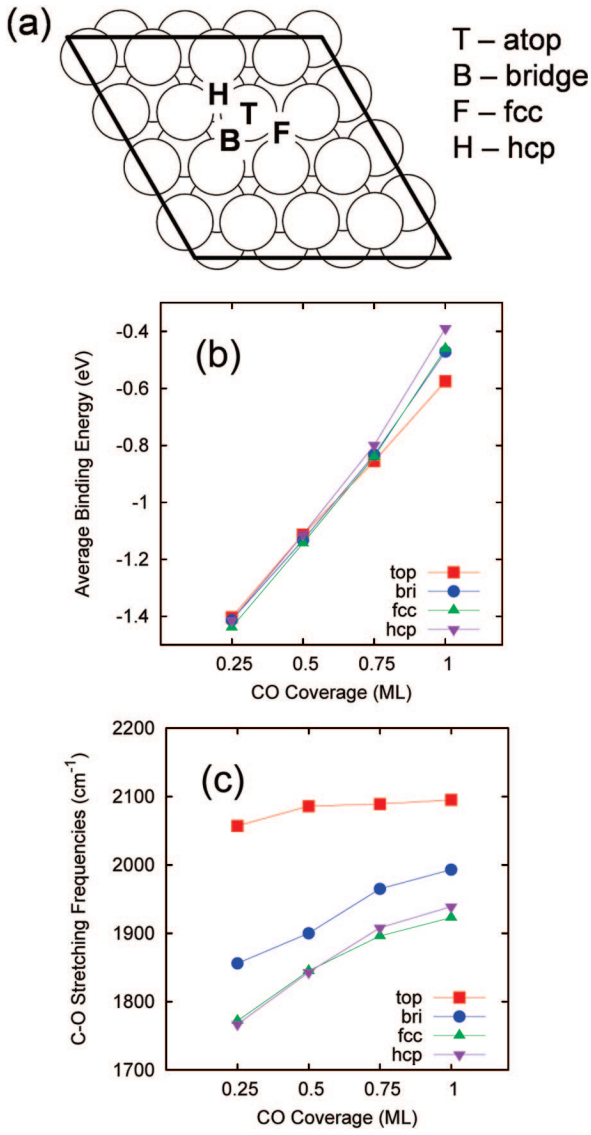

Figure 1. (a) Stable adsorption sites on a Pt(111) surface, top(T), bridge(B), fcc(F), and Hcp(H). (b) Average binding energy of CO on Pt(111) with regular patterns, for 0.25, 0.50, 0.75, and 1.0 ML, respectively. (c) C−O stretching frequencies corresponding to the different coverages.

force on each atom is less than 0.03 eV/Å. The C−O stretching frequencies were calculated by diagonalizing the mass-weighted second derivative force matrix.

For a p(4 × 4) unit cell, there are 96 total binding sites; 16 top, fcc, and hcp sites, and 48 bridge sites. To more efficiently explore the configuration space of CO adsorption, we used classical Monte-Carlo simulations with the Metropolis algorithm[22] to search for the energy minimum. We deposited an initial random configuration of CO molecules within the unit cell. A periodic boundary condition was invoked, and each CO molecule feels the interaction from all neighbors within a cutoff distance of 6 Å. Then adsorbed CO molecules were then allowed to jump to an empty site at random. The total energy before and after the jump is evaluated, and the movement is either accepted or rejected according to the Metropolis algorithm.[22] Each MC simulation was run for 10 million steps, during which multiple temperature ramps between 10 and 2000 K are applied to avoid trapping of the configuration into local minima. The minimum energy configurations from the MC are recorded and shown in Figure 4. Below we mostly focus on the lowest energy state at each surface coverage.

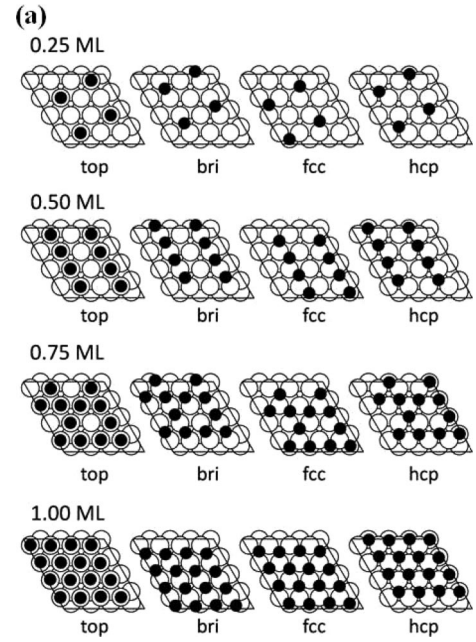

Figure 2. (a) CO adsorption with fixed patterns at 0.25 ML, 0.5 ML, 0.75 ML, and 1 ML, respectively. All COs occupy the same type of site in each adsorption configuration.

Results and Discussions

CO Adsorption with Fixed Patterns. We first studied the adsorption of CO molecules in a p(4 × 4) surface cell of Pt(111) with certain fixed coverage patterns where CO molecules only occupy one type of sites. Figure 1a shows the four types of stable CO binding sites (top, bridge, fcc, Hcp) on a nondefected Pt(111) surface. With the RPBE functional, the binding energies of those sites on Pt(111) at low coverage of 0.25 ML are 1.40, 1.41 1.44, 1.41 eV, respectively. The energy differences are within 0.1 eV, with fcc adsorption being slightly preferred over top adsorption by 0.04 eV. Adsorption at these stable sites are also calculated at other coverages, with CO being fixed into regular patterns as shown in Figure 2. The adsorption energies, bond lengths, and CO vibrational frequencies are summarized in Table 1 and plotted as a function of CO coverage in Figure 1. As can be seen from the Figure 1b, average CO binding energy decreases from around ∼−1.4 eV at 0.25 ML to ∼−0.5 eV at 1 ML coverage, indicating the existence of a strong lateral repulsion between adsorbed CO molecules. Considering that the magnitude of the lateral interaction is much larger than the energy differences among different sites under low coverage conditions, CO adsorption patterns at high coverage will likely be determined by the lateral interactions from through-space interactions and metal-sharing effects.

The calculated C−O stretching frequencies (ν_{C-O}) are listed in the last column in Table 1. The stretching frequency for the free CO molecule with RPBE functional is 2117 cm^{-1} compared to the experimental value of 2145 cm^{-1}. Upon adsorption, the frequency is lowered because of bond formation between the carbon atom and surface atoms. The coordination-dependence of the CO stretching frequency has been used as a general indicator for adsorption sites in spectroscopy measurements. Our calculated CO stretching frequency under low coverage (0.25 ML) is 2057, 1856, 1772, and 1767 cm^{-1} for CO in top, bridge, fcc, and hcp sites, respectively. This reasonably agrees with experimentally measured frequencies of 2100 and 1850 cm^{-1} for top and bridge sites at similar coverages.[9,23] It can also be noted that with increasing CO coverage, the CO stretching

TABLE 1: Calculated Average CO Adsorption Energies, Bond Lengths, and Vibrational Frequencies at 0.25, 0.5, 0.75, and 1.0 ML Coverage, Respectively

coverage (ML)	adsorption site	average binding energy (eV)	Pt−C bond length (Å)	C−O bond length (Å)[a]	C−O vibrational frequency (cm^{-1})[b]
	top	−1.404	1.846	1.158	2057.5
0.25	bridge	−1.413	2.030	1.181	1856.4
	fcc	−1.439	2.128	1.196	1772.7
	hcp	−1.414	2.089	1.194	1767.4
	top	−1.113	1.848	1.161	2086.6
0.50	bridge	−1.133	2.031	1.175	1911.2
	fcc	−1.144	2.161	1.186	1845.7
	hcp	−1.113	2.115	1.186	1843.9
	top	−0.855	1.854	1.160	2089.5
0.75	bridge	−0.833	2.046	1.179	1965.5
	fcc	−0.840	2.121	1.182	1896.4
	hcp	−0.799	2.126	1.182	1908.1
	top	−0.575	1.860	1.160	2095.8
1.0	bridge	−0.471	2.066	1.172	1993.3
	fcc	−0.461	2.151	1.179	1923.4
	hcp	−0.389	2.152	1.178	1939.0

[a] The C−O bond length in an isolated CO molecule is 1.143 Å. [b] The stretching frequency of an isolated CO molecule is ν 2117. [c] m^{-1}.

TABLE 2: Classical Potential Energy Function Parameters, Binding Energies, α (eV), and β (Å)[a]

	ΔE_{top}	ΔE_{bri}	ΔE_{fcc}	ΔE_{hcp}	α	β	R^2	rms	no. of config
Model I[a]	−1.404	−1.413	−1.439	−1.414	0.284	2.980	0.985	0.226	13
Model II[b]	−1.442	−1.429	−1.433	−1.395	0.292	2.976	0.996	0.120	13
Model III[c]	−1.418	−1.479	−1.462	−1.423	0.281	2.910	0.994	0.185	39
δ	0.0	0.012	0.007	0.009					

[a] Using DFT ΔE. [b] Fitting all parameters. [c] Including metal-sharing terms. [a] The R^2 and RMS of the resulting fit to the DFT data are included.

frequency blue shifts to higher wave numbers because of weakened CO−Pt bonding. The stretching frequencies of CO in Hcp sites show the most pronounced blue shift, consistent with the observation that CO in the hcp site show the largest decrease in binding energy from low coverage to high coverage.

CO Lateral Interactions on Pt(111). The CO adsorption patterns in the previous section gives us valuable insight into the coverage effect of CO on its binding energies and stretching frequencies. However, such regular adsorption patterns do not necessarily represent the ground-state configuration corresponding to the given coverage. Also, to find a differential binding energy curve with reasonable accuracy, more adsorption configurations at intermediate coverage need to be explored; all these coverage patterns would not look like simple regular patterns we had adopted in the previous section.

To get a realistic representation of the ground-state configuration of CO adsorption at different coverages, we used Monte-Calro simulations with a classical model to predict possible low energy configurations. The classical model was initially parametrized to reproduce the CO binding energies of 16 configurations (Figure 2) at 0.25, 0.50, 0.75, and 1.0 ML coverage. The classical potential energy function we employed in the fit has the following form:

$$E_{tot} = n_A\Delta E^0_{top} + n_B\Delta E^0_{bri} + n_F\Delta E^0_{fcc} + n_H\Delta E^0_{hcp} + \frac{1}{2}\sum_{i,j}^{N} \alpha \exp(-\beta(R_{ij} - r_0)) \quad (2)$$

where ΔE^0 represents the low-coverage intrinsic CO binding energies at the top, bridge, fcc, and hcp sites, and the through-space repulsions between adsorbates are approximated by an exponential term. R_{ij} is the lateral distance between CO molecules. By setting r_0 to the nearest neighbor distance of Pt (2.821 Å), α represents the energy of the CO−CO interaction at two neighboring sites. We initially set ΔE^0 values to DFT adsorption energies at 0.25 ML and fitted the exponential term only (α and β). The resulting model (Model I, Table 2) fits the DFT data with an R^2 of 0.985 and an rms of 0.23 eV. Notable outliers (high energy states of bridge, fcc, and hcp adsorption at 1.0 ML) were excluded in the fit. The model fits the low energy states fairly accurately.

In Model II, ΔE^0 are treated as fitting parameters and are allowed to vary. The parameters change only slightly from those of Model I. The R^2 improves to 0.996 and the rms decreases to 0.12 eV. In Model II, CO top binding energy becomes slightly favored over that of the other sites, because adsorption on the top site is preferred on high coverage configurations. Both Model I and Model II reasonably reproduce the low energy states of CO adsorption. We plotted the strength of lateral interaction from the fit and compared it to the pure lateral interactions of two CO molecules in a vacuum. As we can see from Figure 3, the CO−CO lateral interaction on Pt(111) is stronger than its counterpart in a vacuum. Thus, the parametrized lateral interaction also effectively folds in certain substrate-mediated contributions.

The parameters in Model II had been used in MC simulations to find the lowest energy configuration at intermediate coverages ranging from zero coverage all the way to 1.0 ML. For all the MC simulations, we kept several lowest energy configurations and confirmed their energies with DFT calculations. The lowest energy state among these configurations is taken as the ground state for that particular coverage. The binding energies predicted by the MC simulations and the corresponding DFT energies agree within 0.02 eV/molecule.

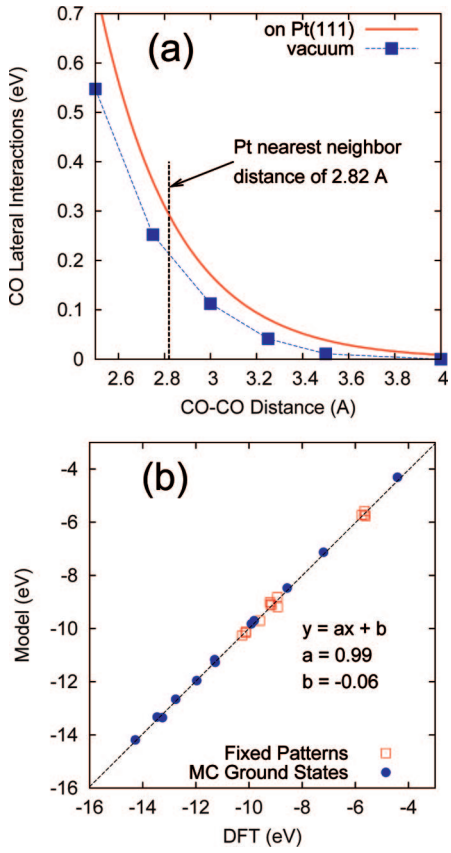

Figure 3. (a) CO lateral interactions on Pt(111) versus in vacuum. (b) Correlation between energies predicted by Model II and DFT energies.

Differential Binding Energies and Comparison to Experiments

The ground-state geometries for the predicted intermediate coverages are shown in Figure 4a. The adsorbed CO is generally uniformly distributed on the surface to minimize their lateral repulsions. By using the p(4 × 4) unit cell, we were able to explore more adsorption patterns than those compatible with a smaller c(2 × 4) or p(2 × 2) unit cells. Our combined MC simulations with DFT verification enhanced our probability of reaching the correct ground state. In one of the previous theoretical attempts to address coverage effect on CO adsorption, Steckel et al.[16] used DFT to investigate the adsorption of CO on partially precovered Pt(111) surfaces. On the basis of a certain set of calculations with fixed adsorption patterns, Steckel reported that 0.50 ML of CO coverage was lower in energy than 0.75 ML, and there is a significant barrier for further CO adsorption. In our MC simulations, we allowed CO molecules to equilibrate on the surface and relax to ground states. We discovered a new hexagonal pattern to be the ground state for 0.75 ML, and it was thermodynamically more favorable than 0.50 ML. Because of the larger CO intermolecular distances in the new configuration, no activation barrier was observed for CO adsorption at 0.75 ML, opposite to what was reported in the previous literature.[16]

By using the Monte-Carlo simulations, we found new adsorption patterns that were different from the fixed patterns where CO only occupies one type of site. At 0.50 ML CO coverage, the lowest energy adsorption configuration we found is an equal mix of top and bridge sites. This stable configuration has been independently confirmed by both STM and electron-energy-loss spectroscopy study of the CO adsorption pattern.[24−26]

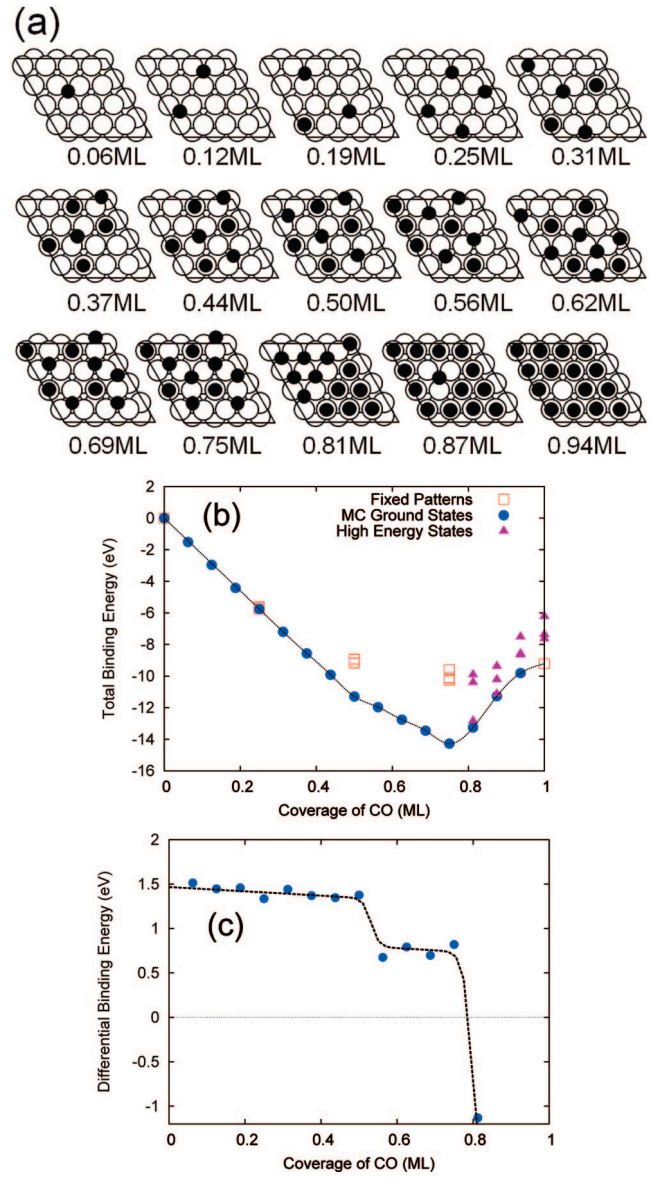

Figure 4. (a) CO adsorption ground states for different coverages from Monte-Carlo simulations. (b) Total energy of the system as a function of CO coverage. (c) Theoretically determined differential binding energy curve of CO on Pt(111). The dotted line is to guide the eye.

Our theoretically determined saturation coverage under 0 K is 0.75 ML. At this coverage, all CO molecules form a uniform hexagonal pattern on the surface with a mixture of top and hollow sites in a 1:2 ratio. This adsorption pattern maximizes the CO intermolecular distances and minimizes the total energy. This adsorption pattern has also been experimentally observed under high pressure scanning tunneling microscopy.[27]

In Figure 4b, we plot the CO adsorption energies as a function of coverage. We can see that under low coverage, each adsorbed CO molecule contributes to a lowering of the total system energy, leading to a linear decrease up to 0.50 ML. Beyond 0.50 ML, some nonlinearity develops because of the lateral interactions between adsorbed CO molecules. The main effect of the lateral interaction is to reduce the CO binding energy, till at around 0.75 ML, it is no longer energetically favorable to add more CO onto the surface. Such behavior is also manifested in Figure 4c, where the differential binding energy curve shows a sudden decrease at 0.50 and 0.75 ML. The sharp decrease in the differential binding energy reflects the relatively

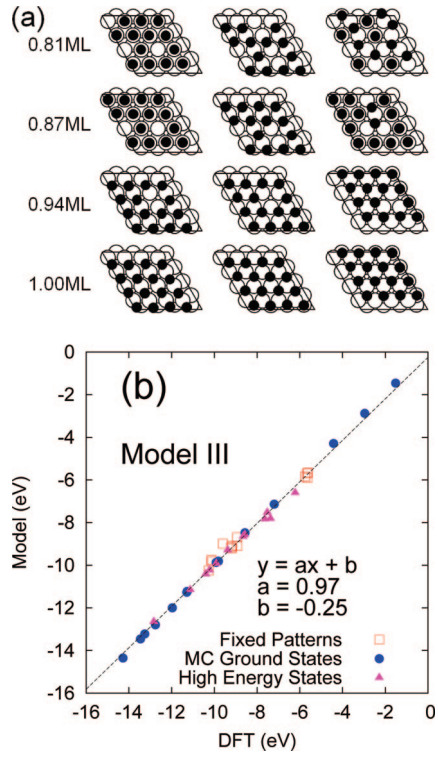

Figure 5. (a) Additional high energy states configurations included in fitting the metal-sharing model. (b) Correlation between model and DFT for Model III.

stable binding pattern at 0.5 ML and a saturation of CO adsorption at 0.75 ML, which has also been observed experimentally.[3]

Model Improvement. In Models I and II, some of the high energy configurations were notable outliers in the fit. This is likely due to the effects of metal sharing. It is possible to quantitatively predict these higher energy states by extension of the current model. To estimate the magnitude of metal-sharing effect, we calculated three high energy configurations at each coverage of 0.81, 0.87, 0.94, and 1.0 ML. These configurations with high CO coverage are expected to exhibit a considerable metal-sharing effect due to a very crowded surface. Their energies are indicated by triangles in Figure 4b. With these additional configurations (Figure 5), we constructed Model III, in which an energetic penalty δ for metal−metal sharing is explicitly included. The form of the new classical potential is:

$$E_{tot} = n_A\Delta E_{top} + n_B\Delta E_{bri}(N) + n_F\Delta E_{fcc}(N) + n_H\Delta E_{hcp}(N) + \frac{1}{2}\sum_{i,j}^{N}\alpha\exp(-\beta(R_{ij} - r_0)) \quad (3)$$

where $\Delta E_i(N) = \Delta E_i^0 + N\delta$, i = bri, fcc, and hcp, N is the number of neighboring COs sharing at least one metal atom (d < 3.0 Å), and the other parameters have the same meaning as in Models I and II. The model fits the DFT data well across 35 different configurations with a rms deviation of 0.18 eV. Table 2 summarizes the fitted parameters and the statistical quality of Model III. The main improvement in including six additional parameters for metal sharing is the better agreement of high energy states. It does not influence the results of our MC ground-state geometries.

Conclusions

While the adsorption of CO on a clean Pt(111) surface has been extensively studied using first-principles calculations, only very few theoretical attempts have been made to explore the coverage-dependent CO binding energies. In this work, we present a systematic first-principles density functional theory study of the coverage-dependent binding energies and equilibrium CO adsorption patterns on Pt(111) over a range of coverages. The search for ground-state CO adsorption patterns is assisted with an empirical lateral interaction model and MC simulations. Because of through-space repulsion and the substrate-mediated metal-sharing effect, CO binding energies show a strong coverage dependence. The theoretically determined CO saturation coverage and differential binding energy curve on Pt(111) agree well with experiments. A useful extension of this work would be to use the parametrized CO lateral interaction model in a kinetic Monte-Carlo simulation to elucidate the effect of coverage-dependent CO binding energies in a reaction environment.

Acknowledgment. We thank Prof. Matt Neurock, and Prof. Enrique Eglesia for fruitful discussions.

References and Notes

(1) Berlowitz, P. J.; Peden, C. H. F.; Goodman, D. W. *J. Phys. Chem.* **1988**, *92*, 5213–5221, Times cited: 124.
(2) Burnett, D.; Capitano, A.; Gabelnick, A.; Marsh, A.; Fischer, D.; Gland, J. *Surf. Sci.* **2004**, *564*, 29–37.
(3) Ertl, G.; Neumann, M.; Streit, K. *Surf. Sci.* **1977**, *64*, 393–410.
(4) Persson, B.; Tushaus, M.; Bradshaw, A. *J. Chem. Phys.* **1990**, *92*, 5034–46.
(5) Steininger, H.; Lehwald, S.; Ibach, H. *Surf. Sci.* **1982**, *123*, 264–282.
(6) Vestergaard, E.; Thostrup, P.; An, T.; Laegsgaards, E.; Stensgaard, I.; Hammer, B.; Besenbacher, F. *Phys. Rev. Lett.* **2002**, *88*, 259601/1.
(7) Longwitz, S. R.; Schnadt, J.; Vestergaard, E. K.; Vang, R. T.; Laegsgaard, E.; Stensgaard, I.; Brune, H.; Besenbacher, F. *J. Phys. Chem. B* **2004**, *108*, 14497–14502.
(8) Desai, S.; Neurock, M. *Electrochim. Acta* **2003**, *48*, 3759–3773.
(9) Gajdos, M.; Eichler, A.; Hafner, J. *J. Phys.: Condens. Matter* **2004**, *16*, 1141–1164.
(10) Zhang, C.; Hu, P.; Alavi, A. *J. Am. Chem. Soc.* **1999**, *121*, 7931–7932.
(11) Ford, D.; Xu, Y.; Mavrikakis, M. *Surf. Sci.* **2005**, *587*, 159–174.
(12) Petrova, N.; Yakovkin, I.; Ptushinskii, Y. *Low Temp. Phys.* **2005**, *31*, 224–240.
(13) Feibelman, P.; Hammer, B.; Norskov, J.; Wagner, F.; Scheffler, M.; Stumpf, R.; Watwe, R.; Dumesic, J. *J. Phys. Chem. B* **2001**, *105*, 4018–25.
(14) Kresse, G.; Gil, A.; Sautet, P. *Phys. Rev. B: Condens. Matter Mater. Phys.* **2003**, *68*, 734011−4.
(15) Gil, A.; Clotet, A.; Ricart, J. M.; Kresse, G.; Garcia-Hernandez, M.; Rosch, N.; Sautet, P. *Surf. Sci.* **2003**, *530*, 71–86.
(16) Steckel, J.; Eichler, A.; Hafner, J. *Phys. Rev. B: Condens. Matter Mater. Phys.* **2003**, *68*, 085416.
(17) Kohn, W. *Rev. Mod. Phys.* **1999**, *71*, 1253–1266.
(18) Kresse, G.; Furthmuller, J. *Comput. Mater. Sci.* **1996**, *6*, 15–50.
(19) Blochl, P. *Phys. Rev. B: Condens. Matter Mater. Phys.* **1994**, *50*, 17953–79.
(20) Perdew, J. P.; Burke, K.; Ernzerhof, M. *Phys. Rev. Lett.* **1996**, *77*, 3865–3868.
(21) S, K.; Gokhale, A.; Grabow, L.; Dumesic, J.; Mavrikakis, M. *Catal. Lett.* **2004**, *93*, 93–100.
(22) Metropolis, N.; Rosenbluth, A. W.; Rosenbluth, M. N.; Teller, A. H.; Teller, E. *J. Chem. Phys.* **1953**, *21*, 1087–1092.
(23) Seebauer, E.; Kong, A.; Schmidt, L. *J. Vac. Sci. Technol. A* **1987**, 464–8.
(24) Pedersen, M.; Bocquet, M.-L.; Sautet, P.; Laegsgaard, E.; Stensgaard, I.; Besenbacher, F. *Chem. Phys. Lett.* **1999**, *299*, 403–9.
(25) Yeo, Y.; Vattuone, L.; King, D. *J. Chem. Phys.* **1997**, *106*, 392–401.
(26) Froitzheim, H.; Hopster, H.; Ibach, H.; Lehwald, S. *Appl. Phys.* **1977**, *13*, 147–51.
(27) Tang, D.; Hwang, K.; Salmeron, M.; Somorjai, G. *Abstr. Pap. Am. Chem. Soc.* **2004**, *227*, U836–U836.

JP8094962